33rd Annual International Conference of the IEEE EMBS
Boston, Massachusetts USA, August 30 - September 3, 2011

Mapping Small Intestine Bioelectrical Activity Using High-Resolution Printed-Circuit-Board Electrodes

Timothy R. Angeli, Gregory O'Grady, Jonathan C. Erickson, Peng Du, Niranchan Paskaranandavadivel, Ian P. Bissett, Leo K. Cheng, Andrew J. Pullan

Abstract—**In this study, novel methods were developed for the *in-vivo* high-resolution recording and analysis of small intestine bioelectrical activity, using flexible printed-circuit-board (PCB) electrode arrays. Up to 256 simultaneous recordings were made at multiple locations along the porcine small intestine. Data analysis was automated through the application and tuning of the Falling-Edge Variable-Threshold algorithm, achieving 92% sensitivity and a 94% positive-predictive value. Slow wave propagation patterns were visualized through the automated generation of animations and isochronal maps. The methods developed and validated in this study are applicable for use in humans, where future studies will serve to improve the clinical understanding of small intestine motility in health and disease.**

I. Introduction

THE motility of the small intestine is governed by several coordinated mechanisms, encompassing neural, hormonal, and bioelectrical systems. Among these mechanisms, a rhythmic electrical slow wave event, generated and propagated by the interstitial cells of Cajal (ICC) imparts a controlling pattern of myenteric excitability that influences the timing, frequency, and direction of contractions along the small intestine [1]. Clinical interest in evaluating intestinal slow wave propagation patterns has been fuelled by recently discovered associations between aberrant slow wave activity and a range of intestinal disorders, such as ischemia [2], chronic nausea and vomiting [3], and post-surgical dysmotility [4]. However, the mechanisms contributing to normal and abnormal small intestine slow wave pacesetting and propagation remain unclear and controversial.

A substantial barrier to better defining normal and abnormal slow wave patterns has been the technical difficulty of recording and analyzing intestinal slow wave activity. Over the past few decades, studies of intestinal slow wave activity primarily employed linear configurations of relatively few electrodes [5-7]. While these methods enabled an analysis of slow wave frequencies, the small number of electrodes meant a spatial analysis of propagation dynamics, pacemaker behaviors, and wavefront interactions could not be performed. More recently, high-resolution, multi-electrode platforms for mapping gastrointestinal slow waves have been introduced, whereby recordings were obtained from spatially dense arrays of electrodes, to define activation sequences in fine spatiotemporal detail [8]. High-resolution mapping methods have now been productively applied to evaluate gastric electrical activity [9]. However, small intestine high-resolution mapping is currently limited by the lack of suitably curved electrode platforms and deficiency of valid methods for analyzing the vast resultant data sets.

The aims of this study were to develop reliable methods of recording electrical activity *in-vivo* from the small intestine, improve the efficiency of the data analysis process through automation, and use these advances to record and visualize small intestine slow wave propagation dynamics.

II. Methods

A. Animal Preparation

Ethical approval was obtained from the University of Auckland Animal Ethics Committee, and the International Guiding Principles for Biomedical Research Involving Animals were followed. All experiments were performed *in-vivo* on white, female, cross-breed, weaner pigs (n=5; 34.9 ± 0.7 kg). Animal preparation and anesthesia were as previously described [10]. A midline laparotomy was performed to expose the small intestine.

B. Electrode Design and Application Methods

Flexible printed-circuit-board (PCB) multi-electrode arrays, validated for gastric mapping [11], were reconfigured for small intestine recordings. These arrays

Manuscript received March 25, 2011. This work was supported in part by the New Zealand Health Research Council, the NIH (R01 DK64775), the Riddet Institute, the Earle Food Research Fund.

Timothy R. Angeli is with the Riddet Institute, New Zealand, and the Auckland Bioengineering Institute, The University of Auckland, New Zealand (phone: +64 9 373 7599 x89742; fax: +64 9 367 7157; e-mail: tang010@aucklanduni.ac.nz).

Gregory O'Grady is with the Department of Surgery and Auckland Bioengineering Institute, The University of Auckland, New Zealand.

Jonathan C. Erickson is with the Department of Physics and Engineering, Washington and Lee University, Lexington, VA, USA.

Peng Du, Niranchan Paskaranandavadivel, and Leo K. Cheng are with the Auckland Bioengineering Institute, The University of Auckland, New Zealand.

Ian P. Bissett is with the Department of Surgery, The University of Auckland, New Zealand.

Andrew J. Pullan is with the Department of Engineering Science and Auckland Bioengineering Institute, The University of Auckland, New Zealand; Riddet Institute, New Zealand; Department of Surgery, Vanderbilt University, Nashville, TN, USA.

consisted of 0.3 mm diameter gold contacts connected to copper wires, embedded in a polyimide base. The recording head of each individual PCB consisted of 32 electrodes arranged in a 16 x 2 array, with an inter-electrode spacing of 4 mm. This inter-electrode spacing was calculated to be sufficient for recording small intestine slow waves based on the application of the Nyquist theorem, where the electrode spacing should be smaller than half of the signal wavelength [12]. Eight PCBs were used simultaneously in each recording, comprising a total of 256 electrodes configured in a 32 x 8 array and covering approximately 35 cm^2 (Fig. 1).

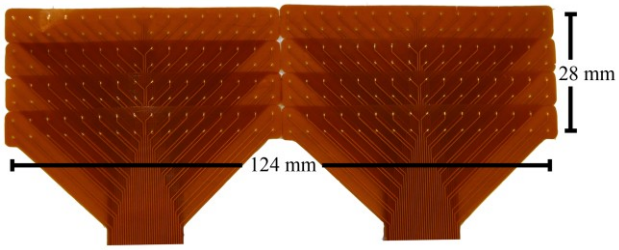

Fig. 1. Flexible printed-circuit-boards (PCBs) were tessellated into an 8 x 32 electrode configuration, encompassing 256 total electrodes with 4 mm inter-electrode spacing.

The PCB arrays were contained in gauze-padded silicone cradles that were sized to match the circumference of the porcine jejunum. The cradled arrays were placed such that the electrodes conformed to the intestinal curvature and covered most of the intestinal circumference, while exerting only gentle pressure on the serosa. Small incisions were made in the mesenteric attachments at the edges of the cradles, through which gauze was strung and tied over the top of the cradles to gently hold them in position during the recordings.

C. Experimental Recording Methods

Serosal high-resolution slow wave mapping was performed where the PCB arrays were placed at intervals along the small intestine of each animal. The first recording was obtained from the duodenum, immediately distal to the pylorus. Then, beginning immediately distal to the ligament of Treitz, five jejunal recordings were taken at one-meter intervals. Two recordings were obtained from the ileum, the first at a distance of nine meters distal to the ligament of Treitz and the second from 10 cm proximal to the ileo-cecal junction. All of the intestinal manipulations were accomplished with the minimum necessary visceral handling. During recordings, the wound edges were approximated and the residual opening packed with warm, saline-soaked gauze to maintain tissue temperature and moisture.

D. Data Acquisition

Data was acquired as previously described [11]. In brief, recordings were acquired using the passive, unipolar ActiveTwo System (Biosemi, Amsterdam, Netherlands). All recordings were acquired at a sampling frequency of 512 Hz. Each recording array was connected via a 1.5 m 68-way ribbon cable to the ActiveTwo System, which was in turn connected to a notebook computer via a fiber-optic cable.

E. Signal Processing and Analysis

Data analysis was performed in the Gastrointestinal Electrical Mapping Suite (GEMS) software v0.6 (Auckland Bioengineering Institute, New Zealand) [13]. All data were first down-sampled to 30 Hz and then filtered using a second order Butterworth filter ('band-pass', 5-60 cycle/min), to filter out low and high frequency noise. Slow wave activation times were then detected using an adapted Falling-Edge Variable-Threshold (FEVT) algorithm, which was recently validated for gastric slow wave event detection [14]. FEVT calculated the convolution of the signal and a falling-edge kernel, and utilized a time-varying threshold for detection of times when the convolved signals exceeded the threshold, effectively identifying the slow wave activation times at the point of steepest negative descent. The FEVT parameters of detection threshold multiplier (η), refractory period (T_r), smoothing kernel width (ρ), and running median window half-width (τ_{HW}), were as previously described in [14] and were re-tuned for use with small intestine data through periodic combination of parameter values listed in Table I. Additionally, the signal transform was also varied between four different methods: Negative Derivative (ND), Amplitude-Sensitive Differentiator (ASD), Non-Linear Energy Operator (NEO), and Fourth-Order Differential Energy Operator (DEO4), as previously described [14].

Parameter values and signal transforms were incrementally varied, and a representative data segment from the porcine jejunum was marked using the FEVT algorithm with each parameter combination. FEVT results were compared to the hand-marked version of the same segment of data to determine true positive (TP), false positive (FP), and false negative (FN) FEVT results. A TP result corresponded to the FEVT mark placed within one second of a hand-marked event, a FP result corresponded to an erroneously placed FEVT mark, and a FN result corresponded to a falsely omitted FEVT mark. Three performance metrics were calculated based on the TP, FP, and FN results, which included sensitivity, positive-predictive value (PPV), and a product of those metrics, A_{roc}, calculated as follows:

$$\text{Sensitivity} = \frac{TP}{TP + FN} \quad (1)$$

$$PPV = \frac{TP}{TP + FP} \quad (2)$$

$$A_{roc} = Sensitivity \times PPV \quad (3)$$

F. Visualization of Slow Wave Activity

All automatically detected slow wave events were manually reviewed, and animations were generated to visualize slow wave propagation. An automated grouping algorithm was then applied to cluster individual slow waves into groups belonging to the same wavefront [15], with manual review of automated results to ensure accuracy. Automated isochronal mapping of activation times [15] was then performed to display and quantify the propagation of successive wavefronts (see Fig. 4).

III. Results

A. Experimental Recording

PCBs were successfully adapted to record *in-vivo* small intestine slow wave activity. Intestinal slow wave activity was readily recorded using the developed methods, and slow wave recordings were of high quality, as shown in Fig. 2.

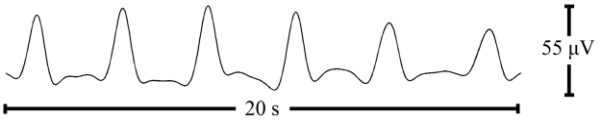

Fig. 2. Sample small intestine slow wave recording from the porcine jejunum, showing six cycles of slow waves from one channel of the PCB. The actual slow wave activation time was defined as the point of steepest negative decent [14].

Preliminary analysis showed that slow wave frequency declined along the length of the intestine from proximal duodenum (17.5 ± 0.7 cycles/min), to mid-jejunum (15.1 ± 0.8 cycles/min; 3 m distal to the ligament of Treitz), to terminal ileum (9.7 ± 0.5 cycles/min). These frequencies are consistent with those previously documented in other species [16].

B. Automated Analysis Algorithm Optimization

Since sensitivity and PPV are inversely correlated, A_{roc} served as the best overall measure of FEVT performance. Following a comparison of the A_{roc} values for each combination of parameter values, an optimal set of parameter values was determined, as shown in Table I.

TABLE I
FEVT Algorithm Parameter Tuning

Parameter	Values Tested	Optimal Value
Signal Transform	[ND, ASD, NEO, DEO4]	NEO
η	[2, 3, 4]	2
T_r	[0.5, 1, 1.5, 2, 2.5] s	2 s
ρ	[0, 1, 2] s	0 s
τ_{HW}	[10, 15, 20] s	10 s

FEVT algorithm parameters are as described in [14]. The parameter values listed in the second column above were systematically combined, tested on an experimental data segment, and results were compared to hand-marked data to evaluate the performance of the FEVT algorithm. Parameter values that resulted in the best performance are shown in the third column.

Channels that did not contain any slow wave signal content ('bad channels'), likely due to poor contact between the electrode and intestinal serosa, were manually screened. After deletion of the bad channels, the performance of the FEVT algorithm demonstrated an A_{roc} value of 0.87. Additional performance metrics are shown in Table II and illustrated in Fig. 3.

TABLE II
Performance Metrics of Tuned FEVT Algorithm

Performance Metric	Value after Tuning
A_{roc}	0.87
Sensitivity	0.92
PPV	0.94
TP rate	0.92
FN rate	0.08
FP rate	0.06

FEVT performance after tuning of the parameters and deletion of channels lacking slow wave signal content. Corresponding parameter values are specified in Table I.

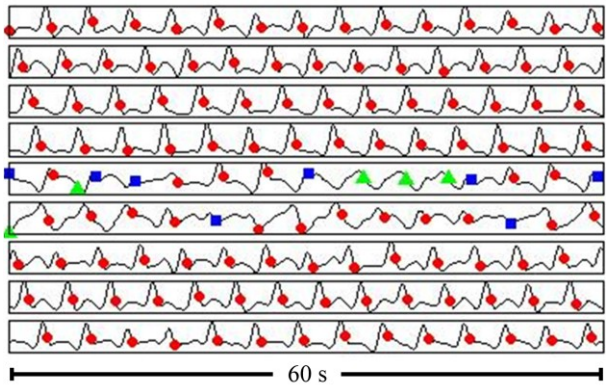

Fig. 3. Sample of nine channels of recorded slow wave activity from the porcine jejunum. Automated slow wave identification from the FEVT algorithm is represented by colored marks. Red circles represent a true positive mark, green triangles represent a false positive mark, and blue squares represent a false negative mark. Amplitude is automatically scaled for each individual channel, but it averaged 36µV in this segment of the intestine.

C. Visualization of Slow Wave Propagation

Activation maps and animations were readily generated, with interpolation for bad channels, as previously defined [14]. Preliminary analysis showed slow wave propagation to be dynamic, with propagation occurring in both the antegrade (Fig. 4a) and retrograde (Fig. 4b) directions. Collisions were often observed between slow waves propagating in opposite directions (Fig. 4c).

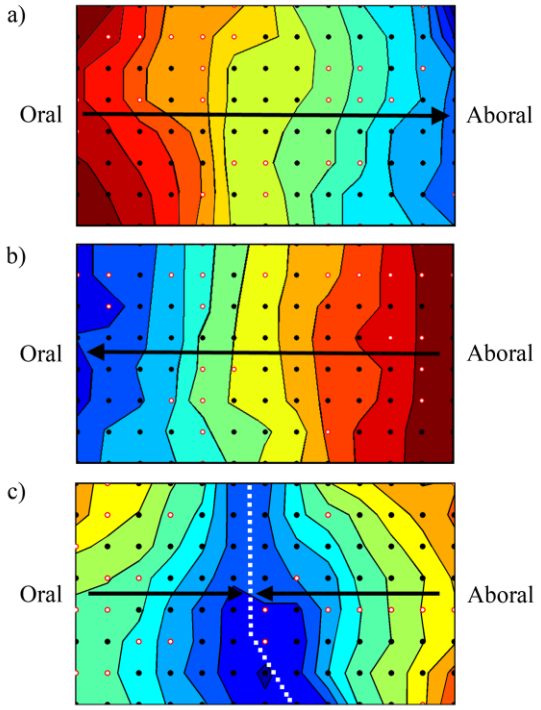

Fig. 4. Isochronal activation time maps of slow wave propagation. The electrode array was wrapped around the circumference of the intestine such that the top and bottom of each map correspond to nearly-adjacent tissue at the mesenteric border. Each activation map shows a single wavefront, with each color band indicating the area of slow wave propagation per unit time, progressing from red (early) to blue (late), reiterated with arrows. Each black dot represents an electrode, and white dots outlined in red represent electrodes where activity was interpolated. (a) Consistent antegrade propagation. Slow wave activity originates oral to the array and propagates antegrade across the array. Each isochronal color band represents 0.5 s. (b) Consistent retrograde propagation. Slow wave activity originates aboral to the array and propagates retrograde across the array. The isochronal spacing is 1.0 s. (c) Colliding slow wave wavefronts. Slow wave activity originates both oral and aboral to the array and collides in the middle of the array, represented by the dashed white line. The isochronal spacing is 0.25 s.

IV. Conclusions

Experimental recording and analysis methods were developed for recording small intestine slow waves, *in-vivo,* in high-resolution. Small intestine slow waves were recorded in a porcine model using the methods that were developed, and slow wave propagation patterns were observed to be variable and dynamic. An automated event-detection algorithm was tuned for use with small intestine recordings and greatly improved the efficiency of data analysis and visualization, which has previously been performed manually in the small intestine.

The methods developed in this study will now allow for comprehensive *in-vivo* studies of small intestine bioelectrical activity. Importantly, these methods are applicable for use in human studies because PCBs can be readily sterilized for human intra-operative use [9]. Future applications of these methods aim to better define organ-level mechanisms of normal and aberrant small intestine bioelectrical activity in human patients, improving the clinical understanding of small intestine motility in health and disease.

Acknowledgment

We thank Linley Nisbet, Dr. John Egbuji, and Dr. Rita Yassi for their technical assistance.

References

[1] J. D. Huizinga and W. J. E. P. Lammers, "Gut peristalsis is coordinated by a multitude of cooperating mechanisms," *Am. J. Physiol. Gastrointest. Liver Physiol.*, vol, 296, pp. 1-8, 2009.

[2] S. A. Seidel, S. S. Hegde, L. A. Bradshaw, J. K. Ladipo, and W. O. Richards, "Intestinal tachydysrhythmias during small bowel ischemia," *Am. J. Physiol.*, vol. 277, pp. G993-9, 1999.

[3] C. H. You,W. Y. Chey, K. Y. Lee, R. Menguy, and A. Bortoff, "Gastric and small intestinal myoelectric dysrhythmia associated with chronic intractable nausea and vomiting," *Ann. Intern. Med.*, vol. 95, pp. 449-451, 1981.

[4] P. Morrison, B. W. Miedema, L. Kohler, and K. A. Kelly, "Electrical dysrhythmias in the Roux jejunal limb: cause and treatment," *Am. J. Surg.*, vol. 160, pp. 252-256, 1990.

[5] W. Alvarez and L. Mahoney, "Action currents in stomach and intestine," *Am. J. Physiol.*, vol. 58, no. 3, pp. 476-493, 1922.

[6] R. A. Hinder and K. A. Kelly. "Human gastric pacesetting potential: site of origin, spread, and response to gastric transection and proximal gastric vagotomy," *Am. J. Surg.*, vol. 133, pp. 29-33, 1977.

[7] J. H. Szurszewski, L. R. Elveback, and C. F. Code. "Configuration and frequency gradient of electric slow wave over canine small bowel," *Am. J. Physiol.*, vol. 218, pp. 1468-1473, 1970.

[8] W. J. E. P. Lammers, A. al-Kais, S. Singh, K. Arafat, and T. Y. el-Sharkawy. "Multielectrode mapping of slow-wave activity in the isolated rabbit duodenum," *J. Appl. Physiol.*, vol. 74, pp. 1454-1461, 1993.

[9] G. O'Grady, P. Du, L.K. Cheng, J. U. Egbuji, W. J. Lammers, J.A. Windsor, and A. J. Pullan, "origin and propagation of human gastric slow wave activity defined by high-resolution mapping," *Am. J. Physiol. Gastrointest. Liver Physiol.*, vol. 299, no. 3, pp. 585-592, 2010.

[10] J. U. Egbuji, G. O'Grady, P. Du, L. K. Cheng, W. J. E. P. Lammers, J.A. Windsor, and A. J. Pullan. "Origin, propagation and regional characteristics of porcine gastric slow wave activity determined by high-resolution mapping," *Neurogastroenterol. Motil.*, vol. 22, pp. e292-300, 2010.

[11] P. Du, G. O'Grady, J. U. Egbuji, W. J. Lammers, D. Budgett, P. Nielsen, J. A. Windsor, A. J. Pullan, and L. K. Cheng, "High-resolution mapping of in vivo gastrointestinal slow wave activity using flexible printed circuit board electrodes: methodology and validation," *Ann. Biomed. Eng.*, vol. 37, pp. 839-846, 2009.

[12] P. V. Bayly, E. E. Johnson, S. F. Idriss, R. E. Ideker, and W. M. Smith, "Efficient electrode spacing for examining spatial organization during ventricular fibrillation," *IEEE Trans. Biomed. Eng.*, vol. 40, no. 10, pp. 1060-1066, 1993.

[13] R. Yassi, G. O'Grady, N. Paskaranandavadivel, P. Du, T. R. Angeli, L. K. Cheng, A. J. Pullan, and J. C. Erickson, "The Gastrointestinal Electrical Mapping Suite (GEMS): Software for analysing and visualising gastrointestinal multi-electrode recordings," *Am. J. Physiol.*, submitted for publication.

[14] J. C. Erickson, G. O'Grady, P. Du, C. Obioha, W. Qiao, W. O. Richards, L. A. Bradshaw, A. J. Pullan, and L. K. Cheng, "Falling-edge, variable threshold (FEVT) method for the automated detection of gastric slow wave events in serosal high-resolution electrical recordings," *Ann. Biomed. Eng.*, vol. 38, pp. 1511-1529, 2010.

[15] J. C. Erickson, G. O'Grady, P. Du, J. U. Egbuji, A. J. Pullan, and L. K. Cheng, "Automated cycle partitioning and visualization of high-resolution activation time maps of gastric slow wave recordings: the Region Growing Using Polynomial Surface-estimate stabilization (REGROUPS) Algorithm," *Ann. Biomed. Eng.*, vol. 39, pp. 469-483, 2011.

[16] N. E. Diamant and A. Bortoff, "Nature of the intestinal low-wave frequency gradient," *Am. J. Physiol.*, vol. 216, no. 2, pp. 301-307, 1969.